Chalcogenide Letters Vol. 21, No. 7, July 2024, p. 499 - 511

Novel C/MoS_2 hollow nanocomposites enhance lithium storage in battery anodes

J. Liu[a], Y. X. Liu[b], J. N. Ding[b], W. Yan[b], Y. C. Wei[b], J. Xu[*b]
[a] *Changzhou Vocational Institute of Industry Technology, Changzhou, Jiangsu, 213164, P. R*
[b] *School of Physics and Electronic Engineering, Jingjiang College, Jiangsu University, Zhenjiang, Jiangsu, 212013, P. R.*

With society's rapid progress, there is an increasing need for electricity among individuals, but the prevailing source of electricity is still mainly obtained through the burning of non-renewable fossil fuels, which are not renewable and pose serious environmental hazards. Lithium-ion batteries are used widely for excellent rechargeable capabilities and high energy density. Recently, researchers have become increasingly interested in transition metal sulfides owing to their cost-effectiveness and remarkable specific capacity. However, their commercialization has been hindered by the expansion of material volume and low electrical conductivity during charging and discharging. We have successfully designed and synthesized MoS_2 nanosheets loaded on carbon spheres with a 3D hollow structure starting from SiO_2 as a template. Due to the doping of carbon materials and particular 3D hollow structures, the optimal C/MoS_2-0.3 hollow nanocomposites exhibit excellent electrochemical performance. Following exposure to over 900 cycles at a 0.5 A g^{-1} ampere density, the materials exhibited an exceptional 958.50 mAh g-1 reversible capacity, demonstrating their remarkable performance.

(Received April 21, 2024; Accepted July 5, 2024)

Keywords: Lithium-ion batteries, Electrochemistry, Anode material, 3D structure, MoS_2

1. Introduction

The growing need for energy and the increasing societal pressure to protect the environment will result in a sustained upward trajectory of the renewable energy share within the future energy market[1-3]. Battery energy storage, as a crucial means of storing energy, possesses the advantages of cost-effectiveness and high stability, thus playing a significant role in advancing renewable energy development, enhancing energy efficiency, and optimizing the overall energy structure. Because of their lower weight and higher energy storage, lithium-ion batteries have found extensive use in many fields such as portable electronic gadgets, electric vehicles, and systems for storing energy[4,5]. The performance and stability of a lithium-ion battery are closely linked to the materials used for the anode and cathode. In the past, graphite has been conventionally employed as the anode material. Nevertheless, its restricted ability to store lithium, limited lifespan during cycles, and inadequate temperature performance have impeded subsequent advancements in this field. As a result, a major focus of research has been the search for cathode materials in lithium-ion batteries for greater energy

*Corresponding author: xjing@ujs.edu.cn
https://doi.org/10.15251/CL.2024.217.499

storage. In the current study, transition metal sulfides have been identified as the most appealing materials used as anodes in batteries that utilize lithium-ion technology, primarily in light of their demonstrated superiority in terms of cycle stability and specific capacity[6-8]. In recent times, there has been a rise in research on this material due to an increase in the number of researchers studying it. The findings suggest that transition metal sulfide anode materials possess higher storage energy and longer stability than traditional graphite anode materials. Molybdenum disulfide (MoS_2), a type of sulfide belonging to the transition metal group, which has excellent electrochemical properties and is a valuable cathode material for lithium batteries. The stratified configuration of molybdenum disulfide facilitates the insertion and removal of lithium ions within its layers via the charging and discharging processes. MoS_2 exhibits superior specific capacity when compared to conventional graphite anodes while also showcasing improved cycle stability and greater lithium storage capacity. The structure of molybdenum disulfide, however, exhibits greater complexity, presenting challenges such as an unstable crystal lattice and low electrical conductivity[9-11]. Therefore, research in this field holds immense significance. Some scholars have incorporated MoS_2 into carbon materials to create a carbon-based composite material with superior electrical conductivity and mechanical strength, which reaches a state of enhanced electrical conductivity and structural stability when this material is employed as the negative electrode. Chen et al. successfully fabricated composites of MoS_2/C nanofibers through the electrospinning technique and employed them as anode materials. Notably, these composites exhibited remarkable cycling stability while achieving a 0.1 A g^{-1} ampere density, and a 650 mAh g^{-1} reversible capacity[12]. In a recent study, Zhang et al. successfully produced graded porous MoS_2/C composite aerogels using a one-pot method, which could have potential applications in battery anodes. In tests, the aerogels demonstrated impressive results with a reversible 653.2 mAh g^{-1} capacity within 0.1 A g^{-1} ampere density and a 334.5 mAh g^{-1} capacity with 5 A g^{-1}[13]. Hu et al. utilized a straightforward hydrothermal approach to successfully design and synthesize 3D layered PANI nanoflowers. Subsequently, annealing was employed to obtain 3D layered flowered MoS_2/C, which were then applied as anode materials. The distinctive combination of the three-dimensional structure, layered architecture, and expanded interlayer distance of the conducting materials maintained an 888.1 mAh g^{-1} capacity with 0.1 A g^{-1} ampere density, and even achieved a 511 mAh g^{-1} capacity at a 1 A g^{-1}[14].

In another example, Zhang et al. developed a new MoS_2/C composite by utilizing cellulose nanocrystals (CNC) as a carbon source. They achieved simultaneous pre-carbonization of CNC and generation of MoS_2 through a hydrothermal reaction, followed by pyrolysis to synthesize a three-dimensional layered microsphere composed of ultra-thin MoS_2/C nanosheets. It achieves 400 mAh g^{-1} capacity with 0.1 A g^{-1} When used as the material of sodium batteries. Furthermore, the ultra-thin MoS_2/C nanosheets revealed a consistent reversible capacity of around 300 mAh g^{-1} even when subjected to an elevated ampere density of 8 A g^{-1}[15]. Despite the great progress made by previous studies, the design of molybdenum disulfide-based carbon cathode materials with excellent lithium storage performance remains a great challenge to meet the demand for lithium-based rechargeable batteries.

We have effectively developed and produced a range of nanocomposites by incorporating MoS_2 nanosheets onto carbon spheres possessing a three-dimensional hollow structure, utilizing SiO_2 as a template. As a result of the distinctive 3D hollow configuration and the incorporation of carbon materials, there was an improvement in both the electrochemical characteristics and structural durability of composites. As a result, the C/MoS_2-0.3 hollow nanocomposite demonstrated

exceptional electrochemical performance. The material capacity did not decrease, and achieved a capacity of 801.05 mAh g^{-1} with 0.1 A g^{-1}, and reached 610.63 mAh g^{-1} with 2 A g^{-1}. Moreover, following more than 900 extended cycles at 0.5 A g^{-1}, the material represents an exceptionally high reversible capacity of 958.50 mAh g^{-1}. The objective of this chapter is to provide a frame of reference for examining the anode materials employed in lithium-ion batteries.

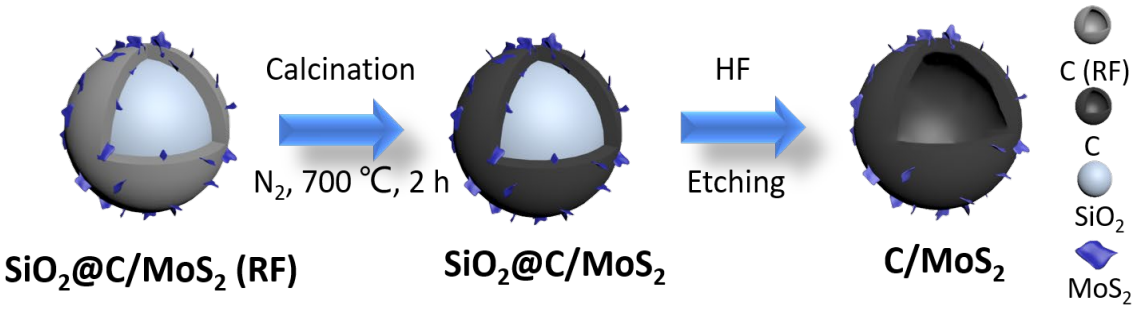

Scheme 1. Composite diagram of C/MoS_2.

2. Experimental

All materials were purchased from Sinopharm, and none of the mentioned samples were further processed.

The synthesis process is shown in Scheme 1. Initially, a compound of 10 ml deionized water (H_2O), 70 ml ethanol (C_2H_6O), 3.46 ml tetraethyl orthosilicate ($C_8H_{12}O_8Si$), and ammonia ($NH_3 \cdot H_2O$) with a mass ratio of 27% was introduced into a 150ml beaker, followed by vigorous stirring at room temperature for 25 minutes. Subsequently, the resulting mixture was supplemented with 0.4g resorcinol ($C_6H_6O_2$) and stirred continuously for an additional period of 15 minutes, after which a drop of formaldehyde (CH_2O) with a concentration of 37% was stirred continuously for 15 minutes after adding. Finally, the suspension was formed by introducing ammonium tetrathiomolybdate weighing at 500 mg to the beaker. The sample was then transferred to a dark environment and stirred for 24 hours. After completing the aforementioned steps, the resulting suspension is transferred to a 100 ml Teflon reactor with stainless-steel cladding and placed in the oven. The reactor is then heated to 200℃ for 24 hours. Once the reactor has attained ambient temperature, The product undergoes multiple rinses using ethanol and distilled water. Finally, it is dried in a vacuum oven set to a temperature of 60°C. The powder obtained after the completion of the aforementioned steps is loaded into a porcelain boat and placed in a nitrogen-filled tube furnace. The temperature is set at 700 °C, 2 °C per minute, and maintained for 5 hours. After cooling, the resulting black powder is subjected to hydrofluoric acid (HF) etching for 24 hours. Subsequently, the sample is washed with pure water until neutralization is achieved. Subsequently, the material is dried in a vacuum oven at 70°C.

The control group consisted of pure MoS_2, which was synthesized by flowing steps:

Dissolve 500 mg ammonium tetrathiomolybdate into 70 ml of water. Subsequently, the solution was transferred to a 100ml Teflon reactor which had been coated with stainless steel, whereupon it was subjected to a reaction at 200 °C and 12 hours. Therewith, the completion of the reaction, allows sufficient time for the reactants to cool down. Then the reactants with three portions

of water and three portions of alcohol, and the final sample was placed overnight in a vacuum oven at 60 °C. The resulting product is a black powder form of pure MoS_2.

The supporting information includes detailed information on the characterization of the material, as well as the electrochemical measurements.

3. Results and discussion

The crystal structure of the product was investigated under different sample ratios during conducting X-ray diffraction (XRD) tests on four samples, namely C/MoS_2(0.1,0.2,0.3,0.4). The obtained test results are presented in Fig. 1a. XRD tests of C/MoS_2-0.3 hollow nanocomposites showed that the peaks located at 33° and 34°, 38.4° and 41.1°, 58.3° and 60.5° corresponding to the (101) and (012), (104) and (015), (110) and (113) crystallographic planes of MoS_2. The diffraction peak positions closely match those listed in the standard PDF card of MoS_2 (JCPDS NO. 17-0744), indicating a high level of agreement[16]. XRD images demonstrate that the position of the diffraction peak remains unchanged when altering the amount of ammonium tetrathiomolybdate. Nevertheless, the relative strength of the diffraction peak at angles of 38.4° and 41.1° increases with the addition of ammonium tetrathiomolybdate. Furthermore, to determine the internal atomic vibration mode of the sample, a laser Raman test was conducted on the C/MoS_2-0.3 sample (Fig. 1b). The G and D bands of carbon materials can be revealed in the Raman spectrum with 1578 cm^{-1} and 1344 cm^{-1} place[17]. Calculating the peaks between D and G is I_D: I_G = 0.89:1, which indicates a high degree of graphitization for hollow carbon spheres in the C/MoS_2-0.3 sample thereby significantly enhancing its conductivity[18].

3.1. Composition and morphology analysis

The C/MoS_2-0.3 material was observed with an electron microscope(SEM and TEM). The characterization results are presented in Fig. 2a. The analysis indicates that the carbon spheres have a 200 nm diameter with a hollow shape, uniform size, and no discernible agglomeration. Furthermore, it has been observed that MoS_2 nanosheets are distributed atop the exterior of the majority of carbon spheres. However, it is noted that some carbon spheres lack MoS_2 nanosheets due to the potential for insufficient addition of ammonium tetrathiomolybdate. This observation is consistent with the findings from transmission electron microscope images shown in Fig. 2b and 2c. Additionally, it was observed that the shell of each carbon sphere possesses a certain thickness through high-resolution transmission image analysis depicted in Fig. 2d, where the shell thickness measures around 15 nm. These partial results collectively demonstrate our successful synthesis of hollow C/MoS_2.

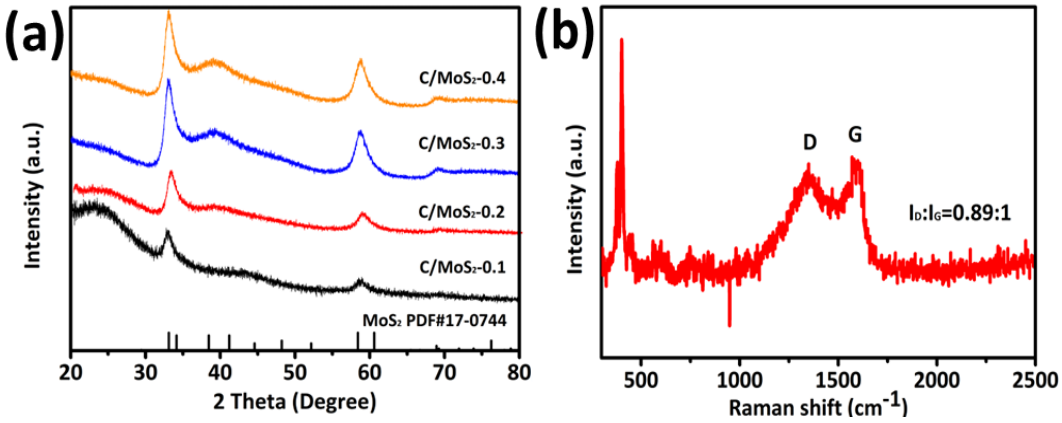

Fig. 1. (a) XRD of C/MoS₂(0.1,0.2,0.3,0.4); (b) Raman result of C/MoS₂-0.3.

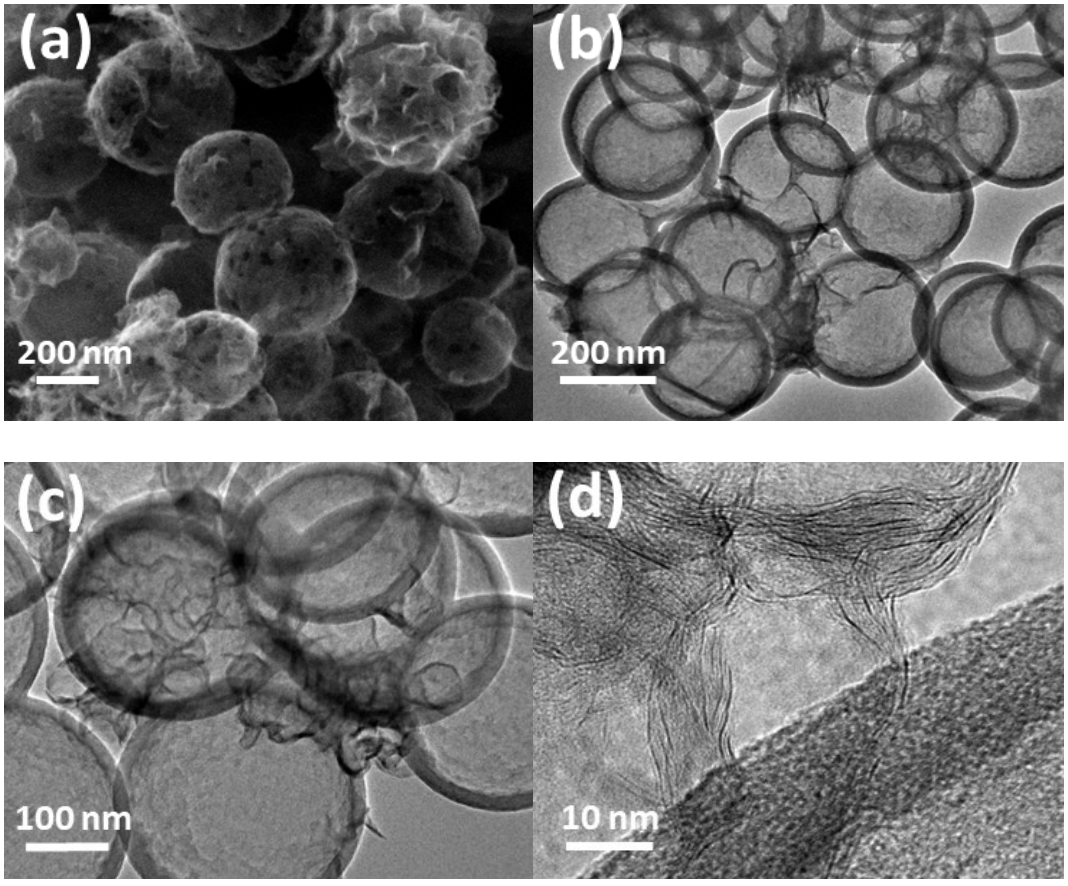

Fig. 2. (a) SEM of C/MoS₂-0.3; (b, c) TEM of C/MoS₂-0.3; (d) HRTEM of C/MoS₂-0.3

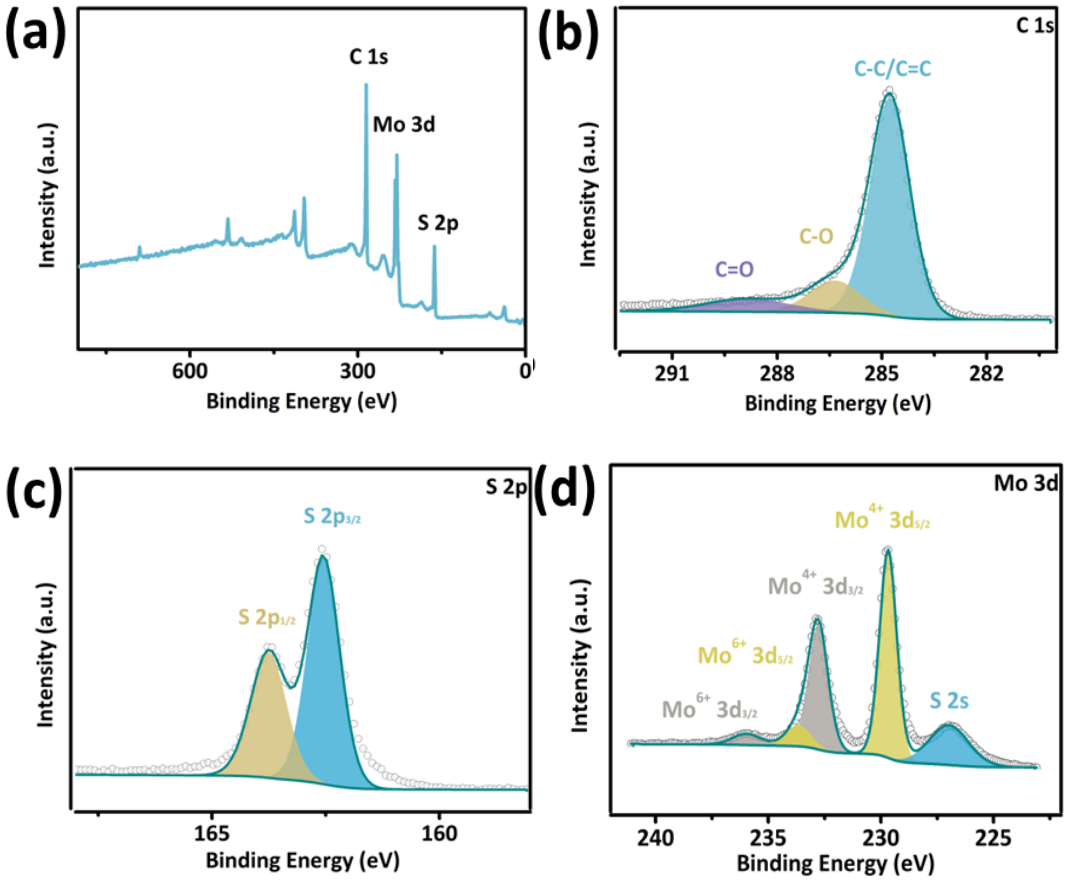

Fig. 3. (a) XPS of C/MoS_2-0.3; (b) high-resolution XPS of C 1s; (c) S 2p; (d) Mo 3d.

The C/MoS_2-0.3 sample was synthesized, and its chemical valency states and primary constituents were examined through X-ray photoelectron spectroscopy (XPS) analysis. Fig. 3a illustrates the complete XPS, existing elements are Mo, C, and S. Fig. 3b illustrates the XPS spectrum of the C 1s region with high resolution, displaying three distinct peaks at energy levels of 288.6, 286.2, and 284.8 eV respectively. These peaks are indicative of C=O bond, O-C bond, and C-C/C=C bond. Fig. 3c illustrates the S 2p high-resolution spectra employed for investigating the electronic state of S in the sample of C/MoS_2-0.3. The S $2p_{3/2}$ and S $2p_{1/2}$ orbitals were linked with the binding energies at 162.5 and 164.1 eV, which indicates that the C/MoS_2-0.3 sample has disulfide bond S^{2-}. This conclusion is by the findings of reference[19]. Fig. 3d demonstrates the existence of distinct peaks observed at energy levels of 229.7 eV and 232.8 eV, which are attributed to Mo^{4+} orbits of Mo 3d. Two additional peaks of 235.7 and 233.5 eV, the composite Mo 3d2/3 and Mo 3d5/2 tracks of Mo^{6+}, respectively. The appearance of Mo^{6+} is caused by the oxidation of MoS_2 samples in the air. Furthermore, small peak at 226.9 eV, which can be attributed to the S 2s peak position[20]. The above analysis further demonstrates our successful synthesis of C/MoS_2.

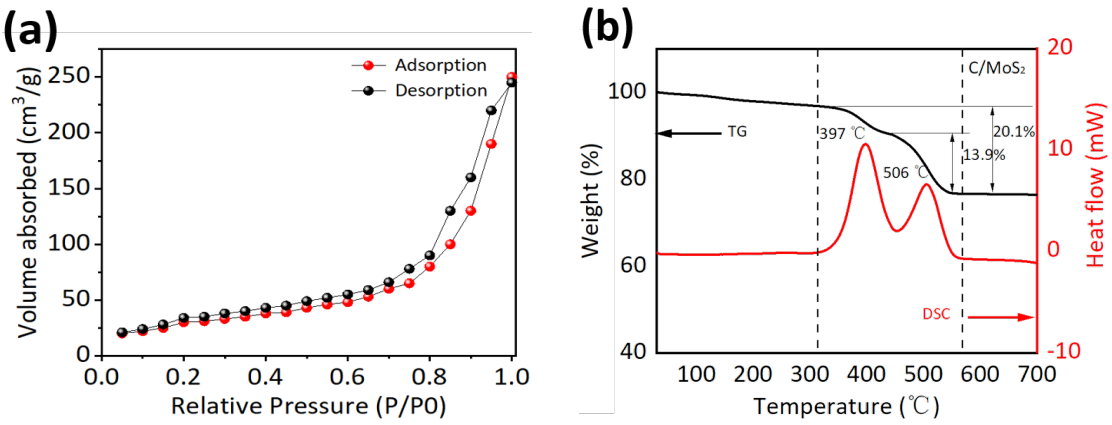

Fig. 4. (a) specific surface area of C/MoS_2; (b) TGA/DSC profile of C/MoS_2.

Fig. 4a presents the nitrogen adsorption analysis results for the synthesized C/MoS_2 nanomaterials. The graph demonstrates the overlapping of the adsorption and desorption curves, suggesting that this material can be classified as a Type I microporous material. It possesses a considerable specific surface area of around 261.6 m^2 g^{-1} and, owing to its hollow sphere configuration facilitates the absorption and storage of electrolytes while promoting the insertion and desorption of lithium ions. The TGA curve reveals that weight loss (C/MoS_2) occurs between two dotted lines, accompanied by an upward peak in the DSC curve indicating an exothermic process of oxidation (Fig. 4b).. At a peak temperature of 397 °C, MoS_2 oxidizes to MoO_3 with a maximum oxidation rate and causes a weight loss of 6.2% for C/MoS_2. Additionally, at a peak temperature of 506 °C, GO undergoes pyrolysis resulting in a weight loss of 13.9% for C/MoS_2. Overall, in the dotted box, a straight drop can be observed due to the oxidation of MoS_2 and the removal of GR.

3.2. Electrochemical measurements

The electrochemical characteristics of the electrode were evaluated by the CV curve. The test results are presented in Fig. 5a. In the cathode scan, two peaks of reduction were identified at 1.0V and 0.47V, which will be discussed in greater detail below. The initial reduction peak arises from the formation of Li_xMoS_2, where Li^+ ions are incorporated into the MoS_2 lattice resulting in a transformation from a triangular prismatic(2H) to an octahedral structure(1T). This reaction can be represented by Eq.(1). The second reduction peak can be ascribed to the formation of Mo and Li_2S, as depicted in Eq. (2)[21]. This reduction peak is absent in the following scans, suggesting an irreversible nature of this reaction. This irreversibility is the production of a solid electrolyte interface film (SEI film) as a result of electrolyte decomposition. In the negative electrode scan, the prominent oxidation peak observed at 2.3V is attributed to Li_2S into S through an oxidation reaction represented by Eq. (3). Furthermore, the minor oxidation peak observed at 1.6V can be attributed to the partial oxidation of Mo, which ultimately results in the formation of MoS_2[22]. The subsequent cathode scan reveals a reduction peak at approximately 1.8V of S to Li_2S. The corresponding reaction formula is depicted in Eq. (3). The observed redox peaks align with the charging and discharging plateaus depicted in Fig. 5b. The scan curves largely overlap in the next two cycle scans, indicating that the composite is highly electrochemically reversible. The relevant conversion equation is shown as follows:

$$xLi^+ + xe^- + MoS_2 = Li_xMoS_2 \quad (1)$$

$$Li_xMoS_2 + (4-x)Li^+ + 4e^- = Mo + 2Li_2S \quad (2)$$

$$\boldsymbol{2Li^+ + S + 2e^- = Li_2S} \quad (3)$$

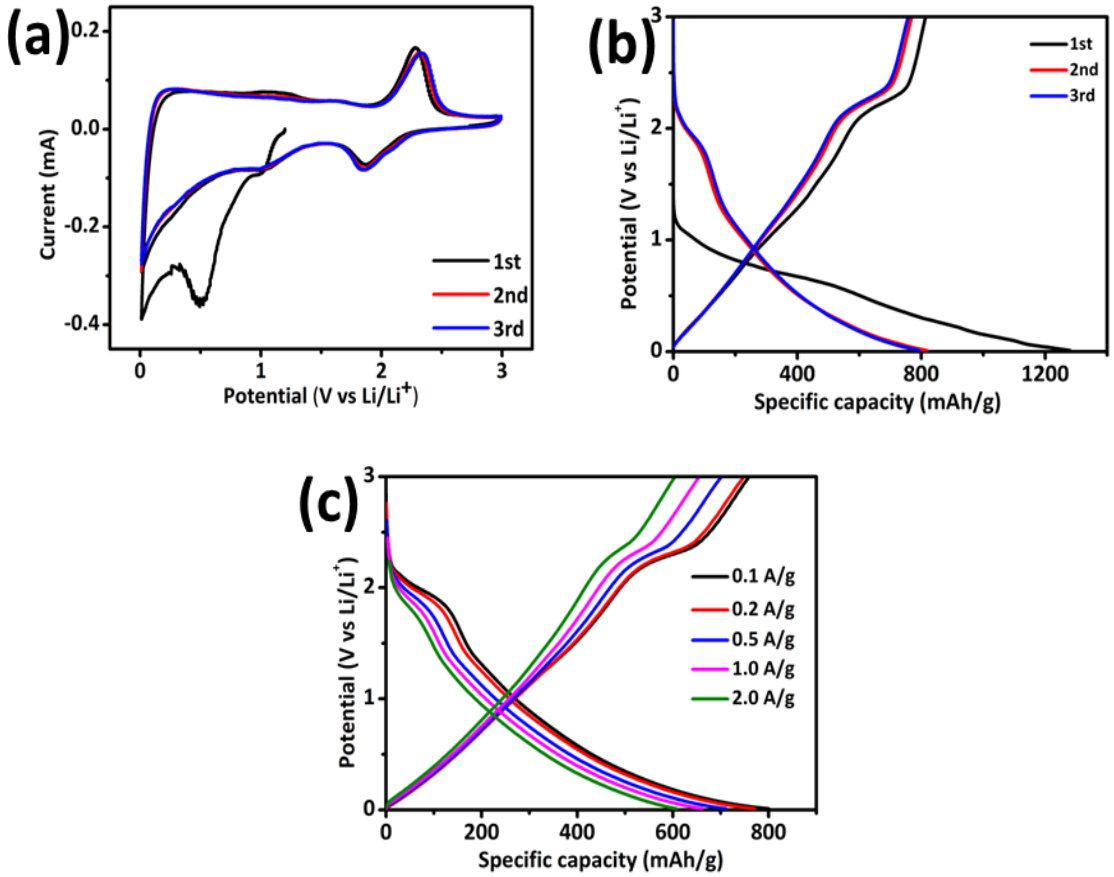

Fig. 5. (a) CV curves of C/MoS_2-0.3 at 0.2 mV s^{-1} for the first three cycles; (b,c) Electrode curves when charge-discharge at (0.1,0.2,0.5,1.0,2.0) A g^{-1}.

The electrodes exhibited near-100% efficiency during the second and third charging and discharging tests, as illustrated in Fig. 5b. This indicates highly efficient charging and discharging processes.

The SEI film formation and slow dissolution of polysulfide intermediates cause the original charge-discharge capacity of 814.04 and 1280.7 mAh g^{-1} for C/MoS_2-0.3. However, the Coulomb efficiency is only 63.6%. In the subsequent cycle test, the battery's charge and discharge curve appear a large overlap, which means an excellent cycle stability of this material. Subsequently, further multiplicative performance tests were performed. we conducted a charge and discharge ratio test wherein the battery demonstrated favorable electrochemical characteristics as the current gradually increased (Fig. 5c). The discharge-specific capacity exhibited minimal decay with increasing ampere density, indicating the sample's low electrochemical polarization and its highly favorable suitability for lithium-ion storage.

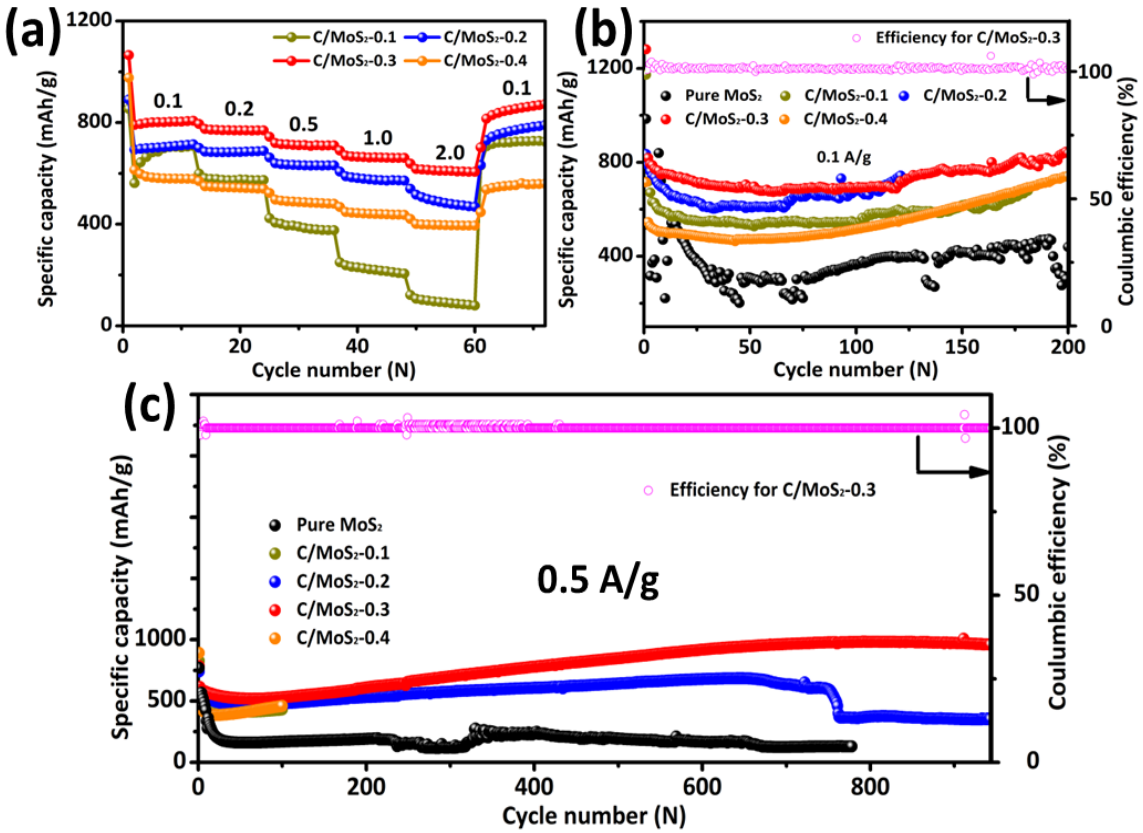

Fig. 6. (a) Distinct discharge capacities of C/MoS_2(0.1,0.2,0.3,0.4) are observed under varying current conditions; (b) cycling efficiency of MoS_2、C/MoS_2(0.1,0.2,0.3,0.4) electrodes under ampere densities of 0.1 A g^{-1}; (c) capacity stability of MoS_2、C/MoS_2(0.1,0.2,0.3,0.4) electrodes under ampere densities of 0.5 A g^{-1}.

At an electric current of 0.1 to 2.0 A g^{-1}, the capacities of C/MoS_2-0.3 are 801.05, 771.94, 715.39, 669.94, and 610.63 mAh g^{-1}. The C/MoS_2-0.1 were 643.30, 581.15, 401.78, 238.10 mAh g^{-1}, and C/MoS_2-0.2 were 693.74, 683.97, 633.62, 579.10, and 493.24 mAh g^{-1} by the same ampere density, respectively (Fig. 6a). The respective values for C/MoS_2-0.4 were 587.44, 548.04, 488.78, 436.60 and 395.16 mAh g^{-1} (Fig. 6a), which were lower than the optimal C/MoS_2-0.3 for all different ratios of samples at all current densities. The discharge-specific capacity of the C/MoS_2-0.3 electrode demonstrated exceptional resilience, rapidly rebounding to 815.31 mAh g^{-1} upon instantaneously reducing the current from 2 A g^{-1} to 0.1 A g^{-1}. The evaluation of the electrochemical performance relies heavily on the cathode material's cycling stability. In comparison to C/MoS_2(0.1,0.2,0.4) electrodes, the C/MoS_2-0.3 electrode demonstrated superior stability and reversible capacity at different currents (Fig. 6b and 6c). It is noteworthy, that the reversible capacity of the C/MoS_2-0.3 electrode remained at 958.50 mAh g^{-1} of 900 long cycles at a current density of 0.5 A g^{-1}, In summary, the C/MoS_2-0.3 electrode exhibits good battery performance due to hollow nanosphere structure and the addition of the appropriate amount of ammonium tetrathiomolybdate.

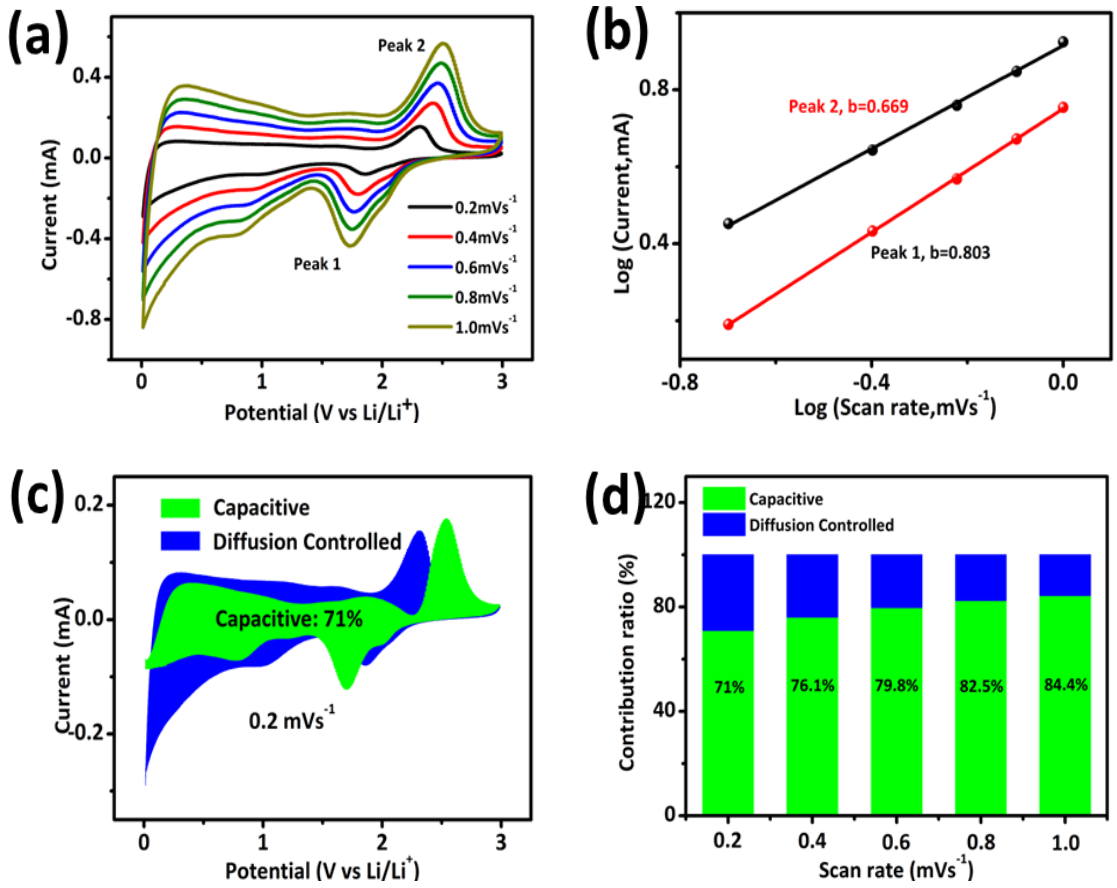

Fig. 7. (a) When the scanning rate of CV curve is 0.2~1.0 mV s^{-1}; (b) Logarithmic function fitting of peak current; (c, d) When the scanning rate of capacitor contribution is 0.2~1.0 mV s^{-1}.

To ascertain whether lithium ions exhibit diffusion or capacitance behavior in the electrodes, CV tests were administered at a range of scan rates, from 0.2 to 1.0 mV s^{-1}, on electrodes containing C/MoS_2-0.3 hollow nanocomposites (Fig. 7a). In this tests, the scan rate is denoted as v, while the currents at different peaks are denoted as I [23]. The correlation between these two variables can be expressed as follows:

$$i = abv \tag{4}$$

$$\log i = b * \log v + \log a \tag{5}$$

$$i(V) = k_1 v + k_2 v^{\frac{1}{2}} \tag{6}$$

The logarithm of Eq. (4) yields Eq. (5), wherein parameter b represents the linear slope of the equation. According to reports, a value of 0.5 for b suggests that the battery's electrode material displays characteristics of diffusion, while a value closer to 1.0 indicates ideal behavior for surface-determined or ideal capacitance-controlled behavior[24]. The fitting results of the two peaks in Fig. 7b, with the b values from 0.5 to 1.0, indicate that the charge and discharge processes consistently demonstrate the presence of both capacitive and cell diffusion characteristics in the electrode. Moreover, the extent of capacitive behavior can be quantified using Eq. (6). The contribution rate of

capacitance is 71% with the scanning speed of 0.2 mV s^{-1} (Fig. 7c). Fig. 7d presents an illustration of the capacitance contribution from the C/MoS_2-0.3 at varying scanning velocities. The results demonstrate that with the increase in scanning speed, there is a gradual enhancement in the contribution of capacitance. This phenomenon facilitates the lithium ions transferring rapidly within the material, thereby enhancing the rate capability and cycling performance[25].

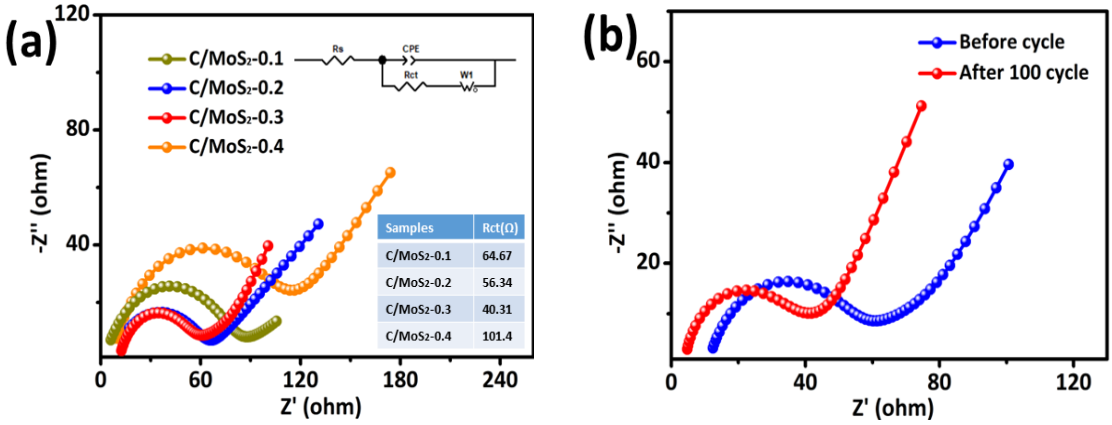

Fig. 8. (a) Comparison of the electrochemical impedance of different samples; (b) C/MoS_2-0.3 electrochemical impedance diagram tested after 100 cycles at 0.1 A g^{-1}.

The reasons for the good properties of C/MoS_2-0.3 hollow nanocomposites were studied, and we analyzed the kinetics of C/MoS_2-0.3 hollow nanocomposites by electrochemical impedance. In Fig. 8a, the semicircular arc is determined by the charge transfer resistance (R_{CT}). Where the R_{CT} is obtained by fitting the diagram of Fig. 8a and inset, the resistance values for C/MoS_2(0.1,0.2,0.3,0.4) are 64.67, 56.34, 40.31, and 101.4 Ω, respectively. As shown in Fig. 8b, after passing 100 cycles the electrode activity was activated and the R_{CT} values showed a decrease. Since the R_{CT} value of C/MoS_2-0.3 is the smallest, it indicates that its charge transfer rate is faster than the other samples and thus has good electrochemical performance.

4. Conclusion

In conclusion, the successful loading of MoS_2 nanosheets on carbon spheres made of SiO_2 as a template was demonstrated by a series of characterizations. These revealed that the electrochemical properties and structural stability of the composites were greatly enhanced due to the unique 3D hollow structure and carbon materials. As a result, the best C/MoS_2-0.3 hollow nanocomposite exhibits excellent electrochemical properties, at 0.1 A g^{-1} ampere density, the battery capacity reaches 801.05 mAh g^{-1}, with minimal capacity decay at high currents (610.63 mAh g^{-1} at 2 A g^{-1}). More interestingly, at 0.5 A g^{-1}, the battery's reversible capacity is 610.63 mAh g^{-1}. Furthermore, a particularly noteworthy achievement was the attainment of a remarkably high 958.50 mAh g^{-1} reversible capacity following the completion of more than 900 ultra-long cycles, with 0.5 A g^{-1} ampere density. Our research findings have the potential to contribute to the advancement of anode materials utilized in Li-ion batteries.

Acknowledgments

This research was supported by the Natural Science Foundation of Jiangsu Province (BK20230521), the Changzhou Basic and Applied Research Project (A023122), and PhD Fund Project (J022008).

References

[1] Wang Y, Yan Q, Luo Y, et al., Renewable Energy, 2023, 210: 1-11; https://doi.org/10.1016/j.renene.2023.04.032

[2] Xu, J; Ye, P; Cheng, Y W, et al., Energy Technology, 2023, 11, 2201452; https://doi.org/10.1002/ente.202201452

[3] Yang Y, Bremner S, Menictas C, et al., Renewable and Sustainable Energy Reviews, 2018, 91: 109-125; https://doi.org/10.1016/j.rser.2018.03.047

[4] Wang Z, Chen Y, Zhou Y. et al., Nanoscale Adv, 2022, 4(20): 4237-4257; https://doi.org/10.1039/D2NA00566B

[5] Galos J, Pattarakunnan K, Best A S, et al., Advanced Materials Technologies, 2021, 6(8); https://doi.org/10.1002/admt.202001059

[6] Wang S, Qu C, Wen J et al., Materials Chemistry Frontiers, 2023; https://doi.org/10.1039/D2QM01200F

[7] Zhou J-E, Chen J, Peng Y et al., Coordination Chemistry Reviews, 2022, 472; https://doi.org/10.1016/j.ccr.2022.214781

[8] Wang J, He J, Omololu Odunmbaku G, et al., Chemical Engineering Journal, 2021, 414; https://doi.org/10.1016/j.cej.2021.128811

[9] Faizan M, Hussain S, Islam M, et al., Nanomaterials (Basel), 2022, 12(12); https://doi.org/10.3390/nano12122008

[10] Faizan M, Hussain S, Vikraman D et al., Journal of Materials Research and Technology, 2021, 14: 2382-2393; https://doi.org/10.1016/j.jmrt.2021.07.127

[11] Liu, M C; Ye P; Wang M; Wang, L L, et al., Journal of Environmental Chemical Engineering, 2022, 108436; https://doi.org/10.1016/j.jece.2022.108436

[12] Chen X, Li L, Wang S et al., Materials Letters, 2016, 164: 595-598; https://doi.org/10.1016/j.matlet.2015.11.079

[13] Zhang Y, He T, Liu G, et al., Nanoscale, 2017, 9(28): 10059-10066; https://doi.org/10.1039/C7NR03187D

[14] Hu L, Ren Y, Yang H, et al., ACS Appl Mater Interfaces, 2014, 6(16): 14644-52; https://doi.org/10.1021/am503995s

[15] Idrees, M.; Amin, B.; Chen, Y P; Yan, X H, et al., International Journal of Hydrogen Energy, 2024, 51: 1217-1228; https://doi.org/10.1016/j.ijhydene.2023.07.222

[16] Xue H, Yue S, Wang J, et al., Journal of Electroanalytical Chemistry, 2019, 840: 230-236; https://doi.org/10.1016/j.jelechem.2019.03.058

[17] Huang Y, Wang Y, Zhang X, et al., Materials Letters, 2019, 243: 84-87; https://doi.org/10.1016/j.matlet.2019.01.141

[18] Cao M, Feng Y, Zhang P, et al., Journal of Alloys and Compounds, 2022, 907; https://doi.org/10.1016/j.jallcom.2022.164499

[19] Hsieh M-H, Li G-A, Chang W-C, et al., Journal of Materials Chemistry A, 2017, 5(8): 4114-4121; https://doi.org/10.1039/C6TA08455A

[20] Liu Y, Zhang L, Wang H et al., Electrochimica Acta, 2018, 262: 162-172; https://doi.org/10.1016/j.electacta.2018.01.023

[21] Pan Y, Zhang J, Lu H., Chemistry, 2017, 23(41): 9937-9945; https://doi.org/10.1002/chem.201701691

[22] Nguyen T M N, Vuong V-D, Phong M T, et al., Journal of Nanomaterials, 2019, 2019: 1-7; https://doi.org/10.1155/2019/8364740

[23] Zhang J, Huang W, Yuan B et al., Solid State Ionics, 2022, 375; https://doi.org/10.1016/j.ssi.2021.115838

[24] Zhong W, Hong J, Wang C, et al., Ionics, 2022, 29(3): 917-930; https://doi.org/10.1007/s11581-022-04866-z

[25] Du X, Huang Y, Feng Z, et al., Materials Chemistry Frontiers, 2022, 6(23): 3543-3554; https://doi.org/10.1039/D2QM00742H